



**HAL**  
open science

## Combining periodic hydraulic tests and surface tilt measurements to explore in situ fracture hydromechanics

Jonathan J Schuite, Laurent Longuevergne, Olivier Bour, Nicolas Guihéneuf,  
Matthew W Becker, Matthew Cole, Thomas J Burbey, Nicolas Lavenant,  
Frédéric Boudin

### ► To cite this version:

Jonathan J Schuite, Laurent Longuevergne, Olivier Bour, Nicolas Guihéneuf, Matthew W Becker, et al.. Combining periodic hydraulic tests and surface tilt measurements to explore in situ fracture hydromechanics. *Journal of Geophysical Research: Solid Earth*, 2017, 122 (8), pp.6046-6066. 10.1002/2017JB014045 . insu-01574812

**HAL Id: insu-01574812**

**<https://insu.hal.science/insu-01574812>**

Submitted on 16 Aug 2017

**HAL** is a multi-disciplinary open access archive for the deposit and dissemination of scientific research documents, whether they are published or not. The documents may come from teaching and research institutions in France or abroad, or from public or private research centers.

L'archive ouverte pluridisciplinaire **HAL**, est destinée au dépôt et à la diffusion de documents scientifiques de niveau recherche, publiés ou non, émanant des établissements d'enseignement et de recherche français ou étrangers, des laboratoires publics ou privés.

## RESEARCH ARTICLE

10.1002/2017JB014045

## Key Points:

- A repeated periodic hydromechanical experiment is performed using surface tiltmeters to measure natural fracture deformation at three depths
- Stacking tilt signals significantly improves signal-to-noise ratios and enables detection of weak stress perturbation in fractures
- No dependence of tilt amplitude on period of test suggests that a fixed portion of fracture deforms regardless of pressure penetration depth

## Supporting Information:

- Supporting Information S1

## Correspondence to:

J. Schuite,  
jonathan.schuite@univ-rennes1.fr

## Citation:

Schuite, J., L. Longuevergne, O. Bour, N. Guihéneuf, M. W. Becker, M. Cole, T. J. Burbey, N. Lavenant, and F. Boudin (2017), Combining periodic hydraulic tests and surface tilt measurements to explore in situ fracture hydromechanics, *J. Geophys. Res. Solid Earth*, 122, doi:10.1002/2017JB014045.

Received 30 JAN 2017

Accepted 14 JUL 2017

Accepted article online 18 JUL 2017

## Combining periodic hydraulic tests and surface tilt measurements to explore in situ fracture hydromechanics

Jonathan Schuite<sup>1</sup> , Laurent Longuevergne<sup>1</sup> , Olivier Bour<sup>1</sup>, Nicolas Guihéneuf<sup>1,2</sup>, Matthew W. Becker<sup>3</sup> , Matthew Cole<sup>3</sup>, Thomas J. Burbey<sup>4</sup>, Nicolas Lavenant<sup>1</sup>, and Frédéric Boudin<sup>5</sup>

<sup>1</sup>Géosciences Rennes, UMR-CNRS 6118, Université de Rennes 1, Rennes, France, <sup>2</sup>Now at G360 Centre for Applied Groundwater Research, School of Engineering, University of Guelph, Guelph, Ontario, Canada, <sup>3</sup>Department of Geological Sciences, California State University, Long Beach, California, USA, <sup>4</sup>Department of Geosciences, Virginia Tech, Blacksburg, Virginia, USA, <sup>5</sup>Laboratoire de Géologie, UMR-CNRS 8538, Ecole Normale Supérieure, Paris, France

**Abstract** Fractured bedrock reservoirs are of socio-economical importance, as they may be used for storage or retrieval of fluids and energy. In particular, the hydromechanical behavior of fractures needs to be understood as it has implications on flow and governs stability issues (e.g., microseismicity). Laboratory, numerical, or field experiments have brought considerable insights to this topic. Nevertheless, in situ hydromechanical experiments are relatively uncommon, mainly because of technical and instrumental limitations. Here we present the early stage development and validation of a novel approach aiming at capturing the integrated hydromechanical behavior of natural fractures. It combines the use of surface tiltmeters to monitor the deformation associated with the periodic pressurization of fractures at depth in crystalline rocks. Periodic injection and withdrawal advantageously avoids mobilizing or extracting significant amounts of fluid, and it hinders any risk of reservoir failure. The oscillatory perturbation is intended to (1) facilitate the recognition of its signature in tilt measurements and (2) vary the hydraulic penetration depth in order to sample different volumes of the fractured bedrock around the inlet and thereby assess scale effects typical of fractured systems. By stacking tilt signals, we managed to recover small tilt amplitudes associated with pressure-derived fracture deformation. Therewith, we distinguish differences in mechanical properties between the three tested fractures, but we show that tilt amplitudes are weakly dependent on pressure penetration depth. Using an elastic model, we obtain fracture stiffness estimates that are consistent with published data. Our results should encourage further improvement of the method.

### 1. Introduction

Fractured geological reservoirs are valued in many environmental and economical engineering projects such as deep nuclear waste storage or fluid and energy production. Therefore, they have been thoroughly studied in the past decades with a broad range of methods involving laboratory, field, and computational experiments [Berkowitz, 2002; Bonnet et al., 2001; Le Goc et al., 2010; Neuman, 2005].

The quest for understanding flow through fractured media, for instance, has mobilized tremendous research efforts because it drives a series of key processes like contaminant and heat transport [e.g., Becker and Shapiro, 2000; Klepikova et al., 2014], underground microbial activity [e.g., Ben Maamar et al., 2015; Pedersen, 1997], or even failure that triggers microseisms or earthquakes [e.g., Cornet, 2016; Guglielmi et al., 2015; Roeloffs, 1988]. Put simply, at the scale of 1 to ~100 m, fractures generally form networks that shape main flow paths in crystalline media. Hydraulic properties of fracture networks depend primarily on their structure and connectivity, which control how easily a fluid particle may find its way through a fractured rock unit [Berkowitz, 2002; De Dreuzy et al., 2001a, 2001b]. Then at fracture scale, flow dynamics are largely controlled by the distance between the fracture's walls, or hydraulic aperture  $a$ , and on the walls' roughness [Renshaw, 1995]. In fact, when a fracture is conceptualized as two parallel plates, the flow magnitude depends on  $a^3$ , known as the cubic law [Boussinesq, 1868; Witherspoon et al., 1980].

Among important processes taking place in fractured reservoirs, the hydromechanical (HM) coupling between pressure-driven flow and fracture deformation has received considerable attention for at least three

reasons. First, it integrates the physical behavior of the fluid and the host rock as a whole, with complex fluid-to-solid and solid-to-fluid interactions [e.g., *Rice and Cleary, 1976; Rutqvist and Stephansson, 2003; Segall, 1992; Slack et al., 2013; Tsang and Witherspoon, 1981; Wang, 2000*]. As an example, a rise in fluid pressure inside a fracture causes reversible deformation when the rock medium can be considered as elastic. This mechanical response can propagate through the rock body faster than fluid pressure diffusion, causing another region of the fracture to contract or dilate. This, in turn, increases fluid pressure at the location and is known as a “reverse response” [see *Slack et al., 2013* as recent example in fractured media]. These type of phenomena may have serious consequences on the interpretation of hydraulic test data as demonstrated by *Vinci et al. [2015]* for instance. Second, the HM coupling has important implications on key hydrodynamical properties. As the fracture’s aperture increases with pressure and given the validity of the cubic law, the flow field might not only be modified, but the stationarity of properties such as transmissivity  $T_h$  and storativity  $S$ , which depend on the fracture’s mechanical state (aperture  $a$  and normal stiffness  $k_n$ ), might be questioned as discussed by *Manga et al. [2012]*, *Murdoch and Germanovich [2012]*, *Shapiro and Hsieh [1998]*, and *Wang and Cardenas, [2016]*. Finally, monitoring reservoir deformation and fluid pressure changes has been proven useful to identify the geometry and estimate HM properties of hydraulically active structures at different scales [*Cappa et al., 2006b; Evans and Wyatt, 1984; Rutqvist, 2015; Schuite et al., 2015*].

Many studies focusing on HM data collection and interpretation with physical models have contributed to describe and comprehend fracture HM processes [*Cornet, 2016; Rutqvist, 2015*]. In particular, sophisticated in situ field experiments involving some controlled water pressure perturbation in a borehole, and the monitoring of fracture deformation by accurate devices, like extensometers, strainmeters, or tiltmeters, have emerged as privileged modus operandi to determine HM properties of fractured reservoirs [*Burbey et al., 2012; Cappa et al., 2006; Guglielmi et al., 2008; Hisz et al., 2013; Rutqvist et al., 1998; Schweisinger et al., 2007, 2009; Svenson et al., 2008*]. For instance, *Schweisinger et al. [2009, 2011]* have evidenced that in the field, the aperture change in a flat horizontal fracture is a hysteretic function of fluid pressure, consistent with results obtained earlier in laboratory stress-strain experiments on rock samples [e.g., *Bandis et al., 1983; Barton et al., 1985*]. In addition, *Schweisinger et al. [2009]* were able to verify that in situ fracture transmissivities  $T_h$  typically decrease when pressure increases during a hydraulic test. Such hydromechanical monitoring complements more classical well tests to enhance constraints on fracture storage [*Burbey et al., 2012; Rutqvist et al., 1998; Schweisinger et al., 2009; Svenson et al., 2008*] by reducing nonuniqueness, even if the nonstationarity of storativity  $S$  during transient pressure conditions is a matter of debate [*Murdoch and Germanovich, 2012*]. Despite these undisputable advances, fracture deformation measurements in these experiments are often performed at the injection source and the fracture inlet itself. Although they are efficient to detect fracture aperture changes, these tests somehow disregard what happens further away from the borehole.

In this paper, we present the development, testing, and analysis of a new in situ hydromechanical experiment implementing ground surface tiltmeters to monitor fracture deformation at depth in response to small amplitude sinusoidal pressure variations at its borehole inlets. This method has five main advantages: (1) in general, periodic pressure variations avoid the massive extraction or injection of water which might be impossible in specific contexts, due to logistical or security issues; (2) controlling the oscillation frequencies enables the recovery of even the weakest signals [e.g., *Bakhos et al., 2014; Renner and Messar, 2006*]; (3) applying various oscillation frequencies allows for sampling different volumes of the subsurface around the tested well, providing a convenient way to assess scale dependencies of key properties [e.g., *Cardiff et al., 2013; Guiltinan and Becker, 2015*]; (4) the small imposed pressure perturbation forms a limited mechanical disturbance on the tested fractures, and therefore, it is safe to assume that the hydrodynamic properties ( $T_h$  and  $S$ ) are not significantly varying due to the hydraulic test itself; and (5) surface deformation monitoring offers a wider—or more integrated—view on the mechanical response of an entire fracture than extensometric measurements at a fracture’s inlet [*Svenson et al., 2008*], even though it is more indirect.

We first introduce the experimental site and setup along with the portable surface tiltmeters. Then, we present the tilt data and the processing strategy employed to optimize signal-to-noise ratios. Finally, we discuss our results and interpret them using a simple mechanical model.

## 2. Material and Methods

### 2.1. Test Site

The experiments were conducted at a small site pertaining to the Ploemeur crystalline aquifer in south Brittany, France (Figure 1), which is part of the H+ hydrogeological network (<http://hplus.ore.fr/>).

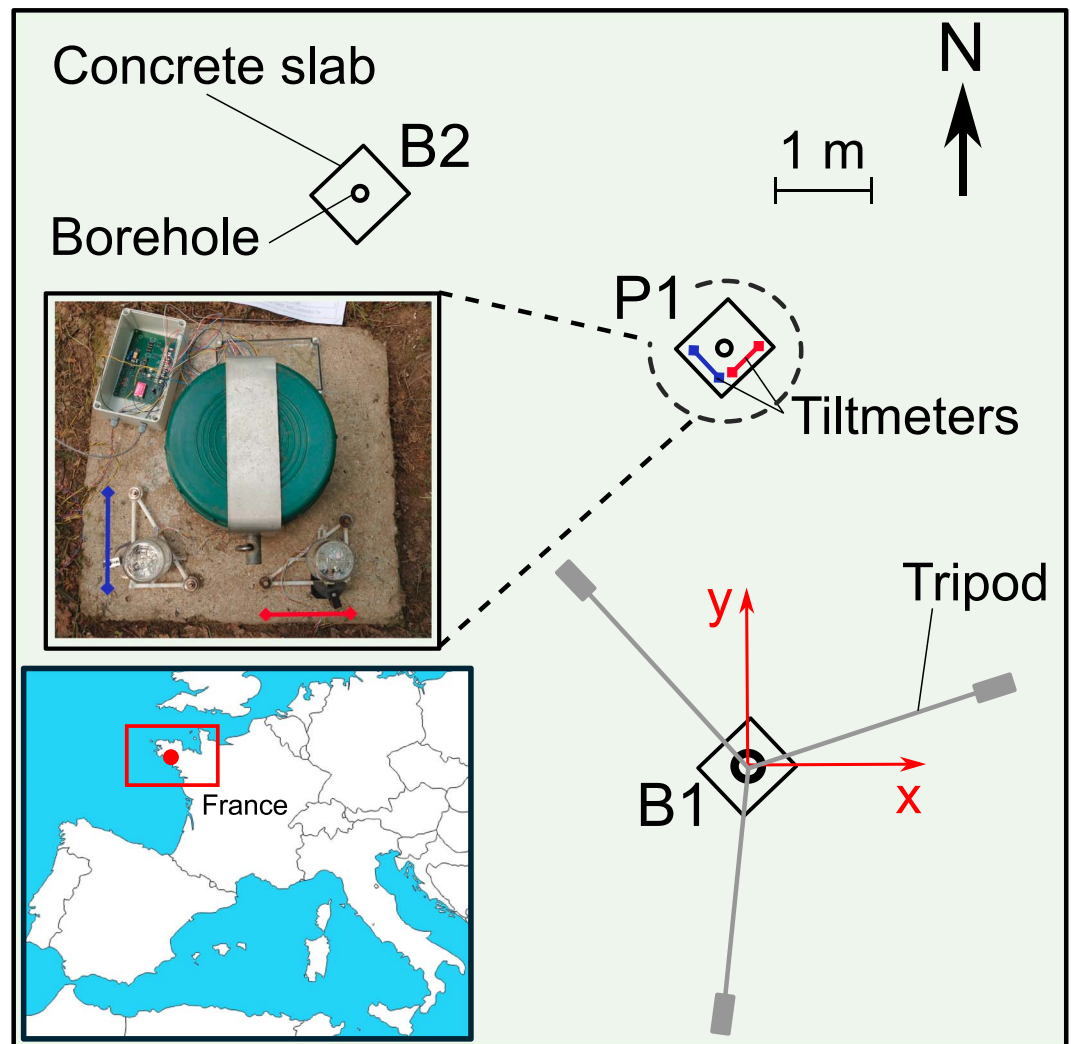


**Figure 1.** Location of the test site (lower left-hand inset) and position of boreholes B1 and B2 as well as the two pendular tiltmeters, oriented N44°E (red) and N145°E (blue).

The experimental site consists of several boreholes a few meters apart from each other and surrounded by woods. Borehole B1 (Figure 1), on which the present work is focused, extends to a depth of 84 m and is uncased from  $z = -23$  m down to its bottom. From optical and acoustic televiewer logging, we observed that B1 crosses first a mica schist unit until  $z \approx -38$  m, then a granitic unit. The contact between granite and the overlying mica schist is nearly horizontal in an area of  $\sim 10$  m around the boreholes (Figure 1) [Le Borgne *et al.*, 2007]. Both rock formations exhibit strong fracturing as numerous open discontinuities are visible from the logs with a density attaining one fracture per meter along most of the borehole's length. However, only four fractures intersecting B1 borehole have been recognized as main and significant transmissive flow paths [Le Borgne *et al.*, 2007]. Furthermore, stochastic inversions of flow tomography experiments [Klepikova *et al.*, 2014] and tracer test data accompanied with ground penetrating radar (GPR) imaging [Dorn *et al.*, 2012, 2013] demonstrated that the catalogued fractures organize into a well-connected network at the interborehole scale. As an illustration, a pathway of 20 m or more between two boreholes should involve at least four fractures according to the estimates by Dorn *et al.* [2013]. These authors also computed a size distribution of these permeable fractures represented as flat disks, with a mean radius of  $5.5 \pm 0.6$  m.

The transmissivity at site scale is fairly high based on classical pumping tests ( $T_h = 10^{-3}$  m<sup>2</sup>/s [Le Borgne *et al.*, 2007]), but Klepikova *et al.* [2014] calculated transmissivities of the fracture system ranging from  $10^{-6}$  to  $10^{-3}$  m<sup>2</sup>/s, which denotes a high degree of heterogeneity. In particular, the few permeable discontinuities intersecting B1 were found to be in the middle and lower transmissivity range of this interval

( $T_h \leq 2 \times 10^{-4} \text{ m}^2/\text{s}$ ). The important features of the three fractures that were hydromechanically tested in the present study are presented in Table 1. Note that these fractures have a relatively low dip, especially B1-3 and B1-4. The fact that they combine both low dip and low permeability guided our choice as to perform the hydromechanical experiment in borehole B1. Indeed, as will be discussed later, the pressure amplitudes induced by the periodic hydraulic tests were expected to be relatively small compared to conventional pumping tests; hence, choosing less transmissive fractures is likely to result in the highest pressure gradients possible, thereby favoring significant deformation. Furthermore, the low dip should optimize the chance to detect the associated fracture deformation by tiltmeters at the surface.

## 2.2. Experimental Setup

The setup for the oscillatory pressure perturbation in borehole B1 consisted of five elements (Figure 2): (1) a double packer apparatus aiming at isolating the desired fracture in the borehole and creating a sealed chamber at its inlet; (2) a cylindrical tank installed in B1 and connected to the chamber by a tube which passed hermetically through the upper packer; (3) a tripod holding a solid cylinder ( $l_c = 2.86 \text{ m}$  in length,  $d_c = 0.07 \text{ m}$  in diameter); (4) a motorized winch able to roll and unroll the wire holding the cylinder, commanded by a computer from which the amplitude and frequency of oscillation can be chosen; and (5) two pressure transducers placed respectively inside the chamber and below, in order to both monitor pressure at the fracture's inlet and verify the packer sealing was effective. A third transducer was placed at the bottom of the cylinder to measure its depth in water. The cylinder's motion causes the water level of the tank to rise and drop periodically, changing the pressure in the chamber accordingly but with some head losses due to viscous dissipation along the downhole tube.

Oscillation periods  $T$  ranging from 15 to 595 s were applied to the cylinder (Table 2). Some oscillation periods were tested two or three times on fracture B1-4 to assess the experimental repeatability. From Table 2, one may observe that pressure amplitudes  $P_c$  reached in the chamber generally increased from B1-4, to B1-2, to B1-3. Note that this is of course an inverse function of fracture transmissivity (Table 1) according to Darcy's law and the mass conservation principle, but it might also be due to different head losses between the surface cylindrical tank setup and the chambers given their different locations in depth. Indeed, the water level in the tank rises up to 1.2 m when the solid cylinder is in its lower end position (Figure 2). Hence, head losses along the vertical tube lie between 0.8 and 1.15 m, thereby representing 67% to 96% of the maximal pressure amplitude reached in the surface tank. As a matter of fact, setting up the experiment was challenging since it required a lot of equipment being installed and secured in a small borehole. Moreover, all pipe connections were custom-made and forced us to use a rather small-diameter downhole tube, which is why head losses are so important. Despite these technical issues, as will be shown hereafter, the water pressure amplitudes achieved in the chamber were sufficient to generate recordable surface deformation.

## 2.3. Tiltmeters

Two portable ground surface tiltmeters (Blum tiltmeters [Saleh *et al.*, 1991]) were used to monitor deformation associated with the oscillatory pressurization of the three aforementioned fractures. Our tiltmeters measure tilt, which is equivalent to the local gradient of vertical displacement in one direction. They were placed onto the concrete slab attached to P1's upper casing in order to optimize coupling between the rock formation and the instruments (Figure 1). Note that during the experiments, borehole B2 was utilized for other monitoring purposes, leaving only P1 available to install the tiltmeter station at about 4 m from B1. Moreover, the shape and orientation of the slab forced us to position our instruments along directions N44°E and N145°E (Figure 1).

The tiltmeters consist of a custom-made horizontal pendulum (Figure 3). They are made of a cylindrical pyrex vessel inside which a silica armature holds a silver mass through two silica fibers of about a hundred microns in diameter. Such thin filaments make the instrument very fragile, but at the same time it enables the pendulum to rotate around its axis with negligible friction. A red diode is fixed on top of the internal armature and continuously lights up a couple of photoelectric cells placed under the pendulum. The silver mass is shaped in such a way that depending on its position, it shades more or less the photoelectric cells from the light source. The shading condition results in differential output voltages given by the cells as a function of the pendulum's position, or in other words, as a function of the inclination of its axis of rotation in one specific direction (see Figure 3). Hence, when the ground tilts, the pendulum starts to oscillate around a new position of equilibrium. Its motion is dampened within 5 s by a magnet placed in front of it during the experiments. As the diode should be the only source of light when recording tilt, the instruments are covered by a polyurethane box that also helps stabilizing the air temperature and shelters them from any significant air motion. In fact,

**Table 1.** Key Features of the Three Lower Permeable Fractures Intersecting Borehole B1

Fracture Label <sup>b</sup>	Depth <sup>a</sup> $z = -d_f$ (m)	Orientation <sup>b</sup> (Strike/Dip)	$T_h^a$ (m <sup>2</sup> /s)
B1-2	50.9	228°/37°	$4 \times 10^{-5}$
B1-3	60.4	220°/31°	$1.3 \times 10^{-5}$
B1-4	78.7	215°/15°	$1.6 \times 10^{-4}$

<sup>a</sup>From *Le Borgne et al.* [2007].

<sup>b</sup>Near-field transmissivity estimated by *Klepikova et al.* [2014].

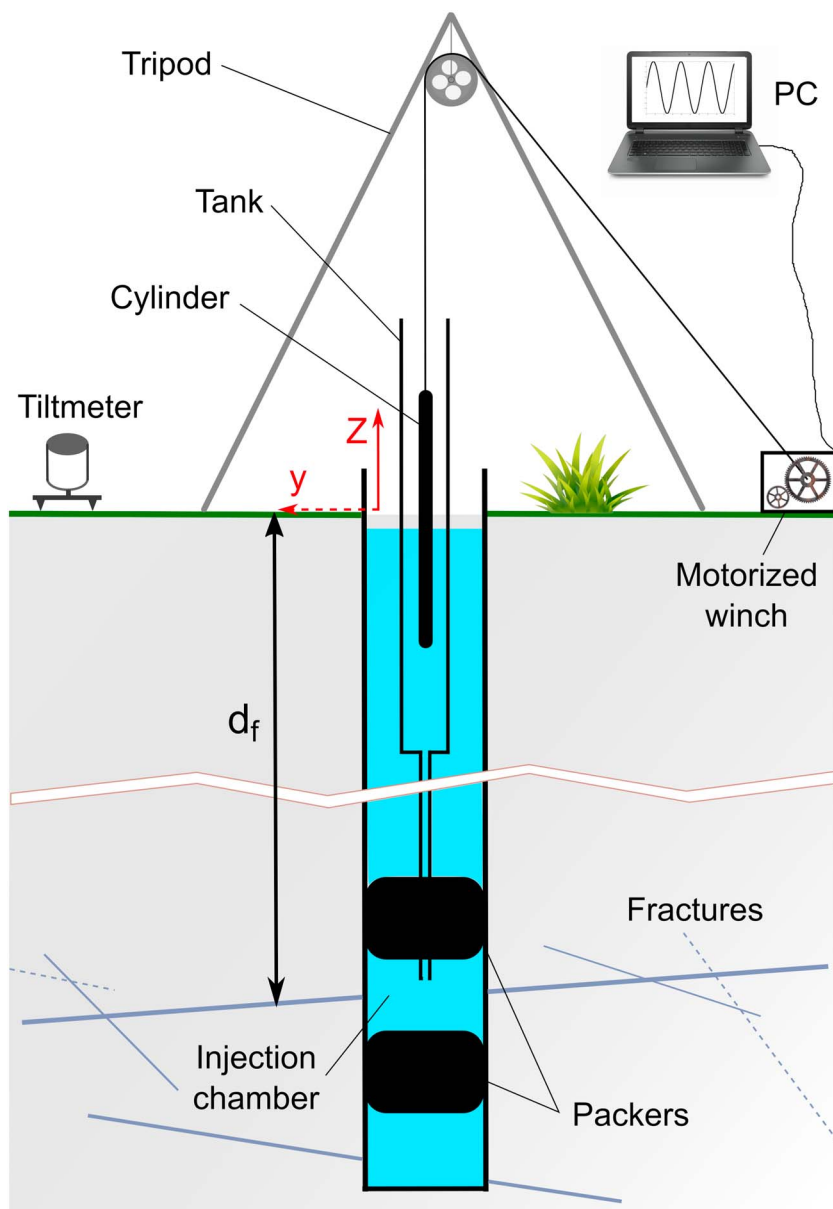


**Figure 2.** Sketch of the experimental setup in and around borehole B1.

**Table 2.** Duration of Tested Periods  $T$ , Number of Complete Cylinder Oscillations (Cycles) for Each Test  $n_p$ , and Associated Pressure Amplitude  $P_c$  Achieved in the Injection Chamber (Figure 2)<sup>a</sup>

Fracture Units	$T$ (s)	$n_p$ (-)	$P_c$ (m)	$\Theta_{44}$ (nrad) <sup>b</sup>	RMSE (nrad) <sup>b</sup>	$\Theta_{145}$ (nrad) <sup>b</sup>	RMSE (nrad) <sup>b</sup>
B1-2	15.0	17	0.12	7.3	1.3	0.0	5.1
	30.9	12	0.32	11.4	2.8	2.6	4.5
	46.4	14	0.28	5.7	3.8	0.9	4.7
	65.5	10	0.33	7.8	5.7	2.4	4.8
	92.6	9	0.33	4.6	9.8	0.2	6.9
	96.0	7	0.14	17.0	10.4	0.0	14.7
	156.7	55	0.01	1.6	3.7	0.0	4.2
B1-3	15.0	16	0.15	7.5	2.2	1.2	1.6
	30.9	10	0.41	11.6	4.7	0.0	3.3
	46.3	9	0.41	12.4	5.3	4.3	4.3
	65.5	10	0.41	7.9	5.1	0.6	5.4
	92.6	9	0.40	11.4	4.4	2.5	4.0
	119.3	9	0.38	10.8	3.0	0.6	3.8
	301.4	27	0.10	8.8	4.6	0.0	2.3
B1-4	15.0	16	0.02	11.0	2.6	0.0	7.6
	30.2	42	0.05	13.5	2.1	0.0	2.0
	30.8	12	0.05	10.7	4.1	1.4	3.4
	30.9	20	0.05	10.9	5.3	3.3	7.2
	46.1	14	0.05	18.0	9.5	0.0	6.4
	46.3	12	0.05	5.8	2.3	0.1	6.3
	46.4	16	0.05	13.0	6.0	1.5	8.5
	65.5	12	0.05	12.4	4.6	8.6	7.0
	65.6	11	0.05	13.8	5.3	3.2	9.5
	67.6	27	0.05	7.2	5.2	0.0	5.0
	92.6	14	0.05	7.8	2.6	0.2	6.4
	92.7	14	0.05	4.8	5.6	3.3	8.9
	95.6	25	0.05	15.9	4.9	2.4	4.1
	114.4	15	0.05	30.9	21.8	0.0	19.1
	115.3	15	0.05	10.0	5.1	0.0	6.3
595.0	10	0.02	8.5	13.5	0.0	14.8	

<sup>a</sup>The last four columns are the observed tilt amplitudes  $\Theta_\phi$  for each of the two tiltmeters installed at the surface with orientation  $N\phi^\circ E$ , and associated root-mean-square error (RMSE).

<sup>b</sup>Stands for nanoradian or  $10^{-9}$  radians.

Blum tiltmeters may be affected by thermomechanical deformation that alters the signal's quality. Nonetheless, diurnal temperature fluctuations occur with a period that is larger than the duration of the typical oscillatory hydraulic tests we conducted.

If  $U$  is the voltage given by the photoelectric cells,  $f_0$  the eigenfrequency of the tiltmeter's pendulum, the tilt  $\theta$  is calculated as

$$\theta = \frac{Uf_0^2}{\Gamma}, \quad (1)$$

where  $\Gamma$  is an amplification factor depending on the instrument's mechanical and electrical characteristics and is determined by calibration in a laboratory. The eigenfrequency  $f_0$  can be determined by monitoring the

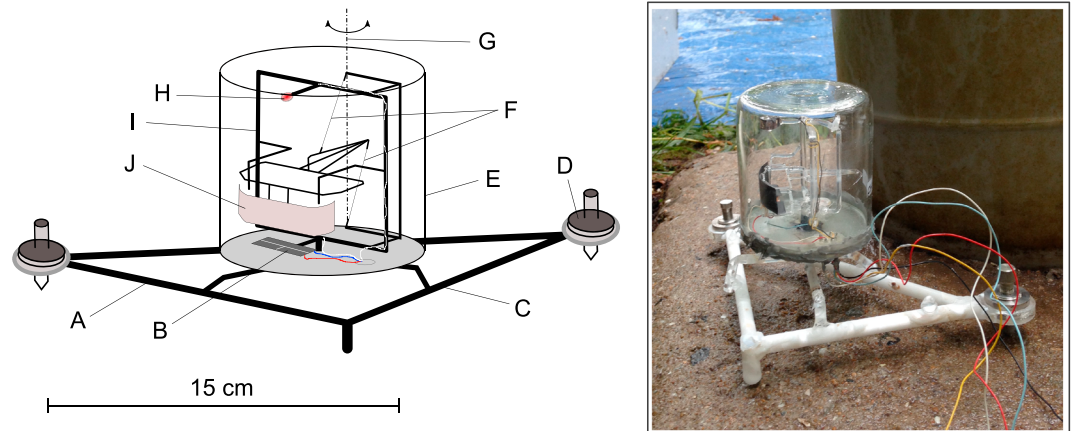


**Figure 3.** Sketch of the (left) Blum pendular tiltmeter and (right) photograph of one of them positioned on a concrete slab before the experiments (right). Meaning of labels: (A) external silica armature and direction of tilt measurement, (B) couple of photoelectric cells for a differential voltage measurement of the light intensity from source in H, (C) External silica armature and direction of period control, (D) Precision adjusting screw, (E) Cylindrical silica casing, (F) Silica fibers holding the pendulum’s mass, (G) Pendulum’s axis of rotation, (H) Red diode, (I) Internal silica armature, and (J) Silver mass of the pendulum.

response of the instrument to a Dirac pulse, which consists of pushing slightly down a screw of the tiltmeter with a finger (Figure 3).

Furthermore, since our tiltmeters are basically pendulums with eigenperiods of  $T_0 = 1/f_0 \approx 9$  s in this case, we can easily describe their motion. For small angular displacements  $q$  of a Blum tiltmeter’s pendulum, the equation of its dampened linear oscillation generated by a ground tilt  $\Omega$  is [Agnew, 1986]

$$\frac{d^2q}{dt^2} + 2\beta\omega_0 \frac{dq}{dt} + \omega_0^2 q = gK_p \Omega \quad (2)$$

where  $\beta$  is the relative dampening coefficient,  $\omega_0 = 2\pi f_0$  is the eigen pulsation of the tiltmeter’s pendulum,  $g$  is gravity acceleration, and  $K_p$  is a coefficient depending on the geometry of the horizontal pendulum. One can show that the transfer function of (2) reads

$$l(\omega) = \left[ -\frac{\omega^2}{\omega_0^2} + 2i\beta \frac{\omega}{\omega_0} + 1 \right]^{-1} \quad (3)$$

Any oscillating system as such experiences a gain in amplitude  $G(T)$  for  $T \rightarrow T_0$  that can be expressed from the modulus of  $l(\omega)$ . The substitution  $\omega = 2\pi/T$  in (3) yields

$$G(T) = \Omega |l(T)| = \Omega \left[ \left( 1 - \frac{T_0^2}{T^2} \right)^2 + \left( 2\beta \frac{T_0}{T} \right)^2 \right]^{-\frac{1}{2}} \quad (4)$$

The value of  $\beta$  has been estimated to about 0.1 for our tiltmeter-magnet couples by analyzing how fast the pendulum’s oscillations is dampened after a Dirac pulse.

#### 2.4. Data Processing

The tilt signal results from a large variety of sources, among which the hydromechanical response of tested fractures might be hidden. These sources may be categorized into two groups: deformation sources and electronic noise. The first ensemble simply refers to any mechanical effect that may cause the ground surface to deform, such as atmospheric loading, the motion of trees generated by wind gusts, or even the steps of staff members working around the field during tests and getting too close to the tilt station. These effects typically occur over a broad range of frequencies, yet larger than  $1/5$  s<sup>-1</sup>. The second group holds all artifacts and irregularities entailed by the electronic equipment used to power the tiltmeters and acquire data. Its signature lies in the high frequencies ( $\geq 1$  Hz), but we took all precautions to limit these effects by using a specific electric source for the tilt station, completely decoupled from other instruments or equipment on the field.

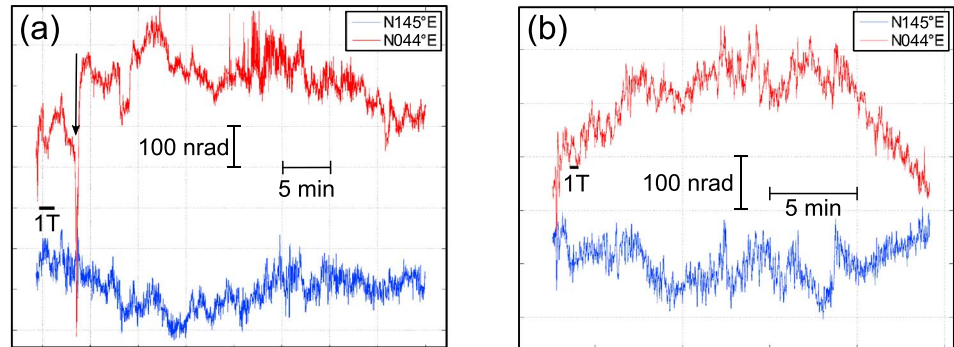


**Figure 4.** Tilt series obtained during two hydromechanical tests on fracture B1-4 ( $d_f = 78.7$  m) at periods  $T$  of (a) 95.6 s and (b) 30.2 s. The black arrow in Figure 4a marks the moment when a staff member passed by the tilt station.

For the sake of clarity, we will here detail our procedure from two consecutive representative examples of oscillatory tests conducted on fracture B1-4. As shown in Figure 4, signals from both tiltmeters experience a variation of 200–300 nrad during a typical oscillatory test lasting 20–40 min. The highest-frequency range is marked by amplitudes on the order of tenths of nrad most of the time, but it occasionally achieves 100–150 nrad with the sudden occurrence of wind gusts which enhance the swaying motion of nearby trees that transmit, through their roots, the energy to ground surface motion. Moreover, one may notice the presence of Dirac pulses from time to time during the experiments. Some of them can be clearly identified as the unfortunate motion of a staff member passing nearby the tiltmeters during a running test (black arrow in Figure 4a). Nevertheless, as will be discussed later on, this can be of some help to assess the mechanical properties of soil.

A common and convenient way to analyze tilt data is to visualize it in the frequency domain [Agnew, 1986]. By calculating the discrete Fourier transform  $\mathcal{F}$  (DFT) of tilt series, it is easier to grasp the signal's structure as a function of frequency. Tilt series are taken as a sequence of  $N$  numbers  $x_0, x_1, \dots, x_{N-1}$  and transformed into a sequence of  $N$  periodic complex numbers as

$$\mathcal{F}\{x_n\} = X_k = \sum_{n=0}^{N-1} x_n e^{-2\pi i kn/N}, \quad k = 0, \dots, N-1. \quad (5)$$

Then, it is possible to recover the amplitude spectral density (ASD)  $\Upsilon(f_t)$  for each frequency  $f_t$  of the tilt signal as

$$\Upsilon(f_t) = \frac{1}{N} \sqrt{\text{Re}(X_k)^2 + \text{Im}(X_k)^2} \quad (6)$$

with

$$f_t = \frac{1}{T_t} = \frac{k f_s}{N} \quad (7)$$

where  $f_s$  represents the sampling frequency.

In Figure 5 we show representative amplitude density spectra of the N44°E tilt obtained from the signal displayed in Figure 4. The strength of recorded signals decays with increasing frequencies up to  $\sim 0.6$  s<sup>-1</sup> (or hertz), following a power law with exponent  $-0.8$ . Note that the power spectrum density (PSD), not shown here, follows an equivalent line of slope  $-2.5$ , typical of fractional Brownian noise or quasi-random walk. One may observe that the ASD deviates noticeably from this line in two instances: first for  $f_t \simeq 0.1$  Hz and second for  $0.2 \text{ Hz} < f_t < 0.4$  Hz, where amplitudes increase significantly. In the first case, the amplitude enhancement is due to the proximity of the tiltmeters' eigenfrequency as can be inferred from their transfer function (magenta lines, Figure 5). The second case is the range corresponding to typical tree sway frequencies in summer, when the experiments were conducted, in agreement with Baker [1997].

Furthermore, for the N44°E instrument, we note a local peak of energy at frequencies corresponding to the cylinder's oscillations. However the amplitude of this peak is not far from that of the high-frequency noise and low-frequency waves, which is why it is not trivial to distinguish the signature of the hydromechanical tests in raw data. It is especially true for the 95.6 s period test (Figure 4a), whereas the well-trained eye could glimpse

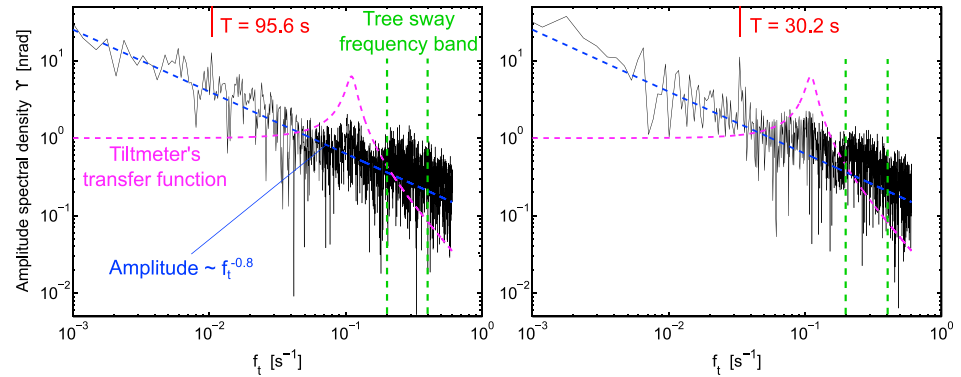


**Figure 5.** Amplitude density spectra (ASD)  $Y(f_t)$  of N44°E tilt series shown in (left) Figures 4a and (right) 4b. The ASD is defined in equations (6) and (7). The tiltmeter transfer function refers to  $l(w)$  defined by equation (3), with  $\beta = 0.1$ .

the 30 s period oscillations in the raw N44°E tilt signal (Figure 4b). As for the N145°E, such peak cannot be clearly detected in the density spectra (data not shown).

In addition, we evaluated the distribution and spread of the tilt series for different frequency ranges. This is a way to evaluate the uncertainty of tilt measurements in relevant frequency bands. As expected from the random structure of the ASD, for each investigated frequency range  $f_t > 1/150$  Hz the distribution of tilt  $\theta$  is gaussian (Figure 6a). Moreover, the standard deviation  $\sigma_\theta$  is consistently increasing with the inverse width of investigated frequency band, that is to say, if  $f_c$  is the high-pass cutoff frequency,  $\sigma_\theta$  increases with  $1/f_c = T_c$  (Figure 6b). In fact, the standard deviation rises sharply up to  $T_c = 30$  s where it generally reaches a value of about 20 nrad and then increases gently toward  $\sim 25$  nrad for  $T_c = 150$  s. Most of the time, the spread of tilt data remains equally consistent between experiments and both instruments (Figure 6b), but exceptions arise when a major Dirac anomaly is present in the data as discussed previously for N44°E series during the 95.6 s test at 78.7 m depth (Figures 4 and 6b). In such cases, the spread is dramatically increased for  $T_c > 10$  s.

In order to recover the tilt amplitudes related to the hydromechanical experiments we employed the stacking technique, commonly used in order to detect weak signals in seismology and enhance the signal-to-noise ratio of geophysical data [Mann et al., 1999; Mayne, 1962; Schimmel and Paulssen, 1997]. We take advantage of the precise knowledge of each hydraulic test's frequency from the analysis of pressure data in the chamber and we fit a sine function to it (Figure 7), of the form

$$P(t)_{x=0} = P_c \sin\left(\frac{2\pi}{T}t + \varphi\right), \quad (8)$$

where  $P(t)_{x=0}$  is pressure in the injection chamber as a function of time  $t$ ,  $P_c$  is its amplitude,  $\varphi$  is the phase, and  $T$ , as previously stated, is the period of oscillation. Then, we cut raw tilt series into  $n_p$  pieces of duration  $T$  and sum up all the pieces together, after linear detrending. By dividing the total summation by  $n_p$ , we theoretically

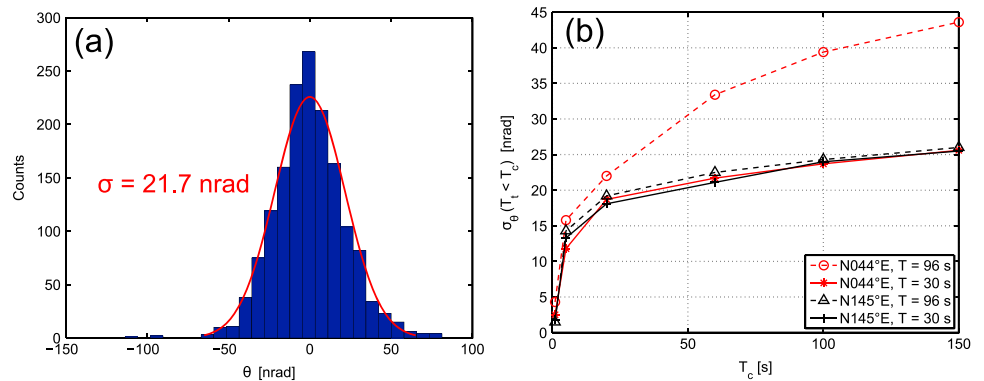


**Figure 6.** Evaluation of distribution and spread of tilt signals. (a) Histogram of tilt values (N44°E) for frequencies  $f_t > 1/60$  Hz and Gaussian fit (in red) and (b) standard deviation  $\sigma_\theta$  as a function of inverse high-pass cutoff period  $T_c = 1/f_c$ .

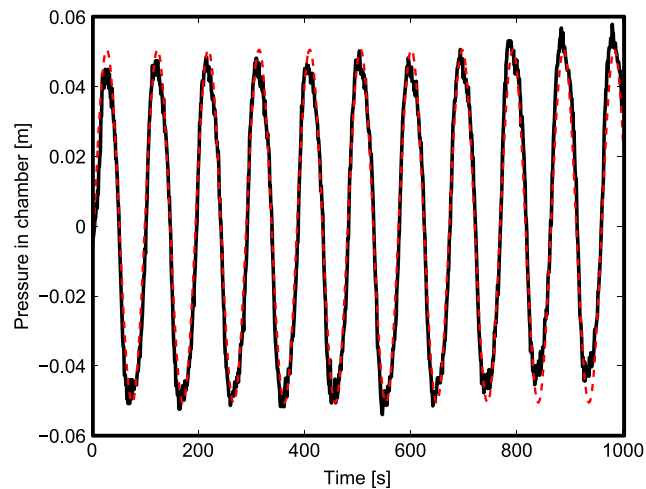


**Figure 7.** Data sample of pressure in the chamber as a function of time (solid black curve) and associated least square fit of a sine function as defined by (8) (dashed red curve).

obtain the characteristic tilt signal associated with the periodic hydromechanical test. In doing so, not only do we improve the signal-to-noise ratio by a maximum factor of  $\sqrt{n_p}$  but also we ensure a correct estimation of the signal's amplitude. As a matter of fact, searching weak signals in an ASD can be biased [Florsch *et al.*, 1995], which is not the case for the stacking method because it has the advantage of conserving any harmonic that could appear if the system's behavior is nonlinear. Here we assume that the noise is homoscedastic so that any fluctuation around the mean targeted tilt signal tends to be canceled out through summation of all  $n_p$  pieces of signal. This means that if  $n_p$  would ideally tend to infinity, the recovered tilt signal due to the hydromechanical test would be, after stacking, a perfect sine function expanding over one period  $T$ .

To further assess the validity of the stacking method in this framework, we tested both stacking and DFT methods on synthetic data where a weak sinusoidal signal of known amplitude and period was hidden in a strong noisy component. Both white and correlated (pink and red) noise were considered. We observed systematically that both methods lead to similar results in terms of amplitude estimates, only when no tapering windows are used prior to DFT calculations, in which case estimates with DFT are significantly biased. However, the main advantage of stacking is that a more objective and easy estimate of the associated error can be performed compared to DFT methods, because no hypothesis on the noise has to be made.

### 3. Results and Interpretation

#### 3.1. Stacked Tilt Signal

Examples of stacked signals are given for each hydromechanically tested fracture in Figures 8–10. Results of all remaining tests can be found in the supporting information. By fitting a sine function to these, we were able to recover the amplitudes  $\Theta_\phi$  for each tiltmeter (results are given in Table 2) and we calculated the associated root-mean-square error (RMSE) as the classical square of the sum of squared differences between model fit and data, divided by the number of data points.

As expected from the density spectrum analysis, only the N44°E instrument seems to encompass a sinusoidal signature of the imposed oscillations. Dispersion of data around the fitted sine is variable: it is in general increasing with test period  $T$ . Nevertheless, the periodic signal is nearly always distinguishable in N44°E times series. The other one, however, N145°E, fails to capture it. Indeed, when N44°E stacked signals usually reveal amplitudes of about 10 nrad for most tested periods, N145°E generally shows flat responses with varying residual noise. We constrained the phase of the N145°E signal to the one of N44°E when fitting the sine functions shown in Figures 8–10. Such a constraint is only hypothetical and is based on the assumption that the pressure diffusion is isotropic in the fractures. Note that the phase of the N44°E signal was not constrained at all.

Given the retrieved amplitudes in N44°E data ( $\sim 10$  nrad), which are less than half the standard deviations at these frequencies (Figure 6b), we demonstrate that we were able to go below the detection limit of our instruments thanks to the periodic nature of the experiment combined with a straightforward processing

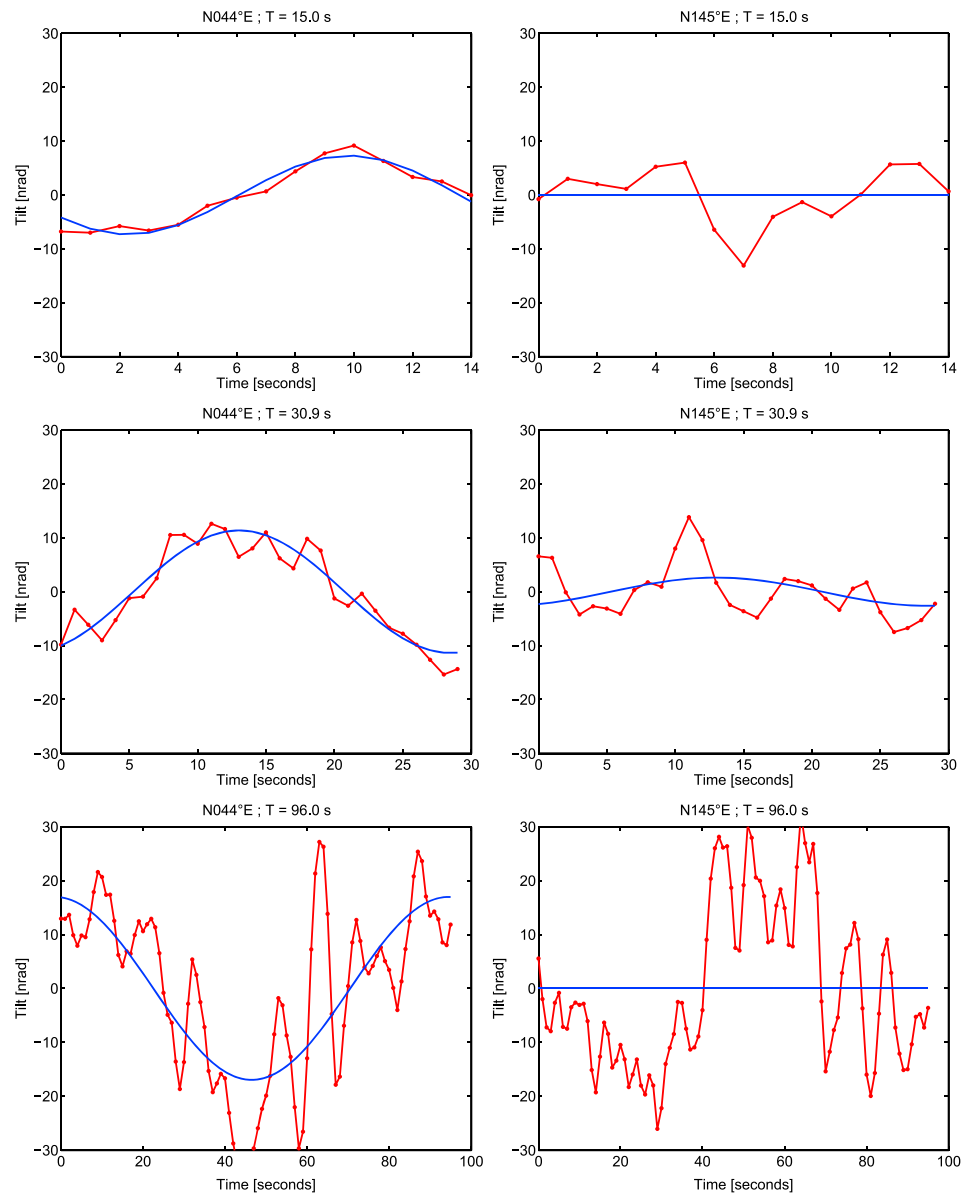


**Figure 8.** Stacked tiltmeter responses for three periodic hydromechanical tests performed on fracture B1-2 ( $d_f = 50.9$  m) in red and associated sine fit of amplitude  $\Theta$  and period  $T$  in blue.

technique. In addition, we compared phase estimates from N44°E tilt and pressure records in the chamber and found no significant difference (not shown here), although admittedly, some difficulty in the comparison arose due to clock drifting issues between the separate acquisition systems for pressure and tilt, as well as fairly large errors in fitting sine functions to the stacked tilt data (Table 2).

### 3.2. Assessing Possible Side Effects in Tilt Data

Monitoring hydromechanical experiments from the surface is challenging because Blum tiltmeters are very sensitive to various sources of perturbation, and in our case, the solicited fractures are rather deeply located in comparison with the scale of the site. If the presence of an intentionally induced mechanical signal is measured by the N44°E instrument, we should mention that there are two potential sources acting at the chosen oscillation periods: the first is the targeted hydromechanical signature of pressurized fractures and the second is the action of the experimental setup itself on the ground surface. In fact, when the cylinder moves up and down the water-filled tank beneath it (see Figure 2), it experiences a buoyant force counteracting its own weight according to Archimedes' principle. This force  $F_s$  varies with the same frequency as the cylinder's

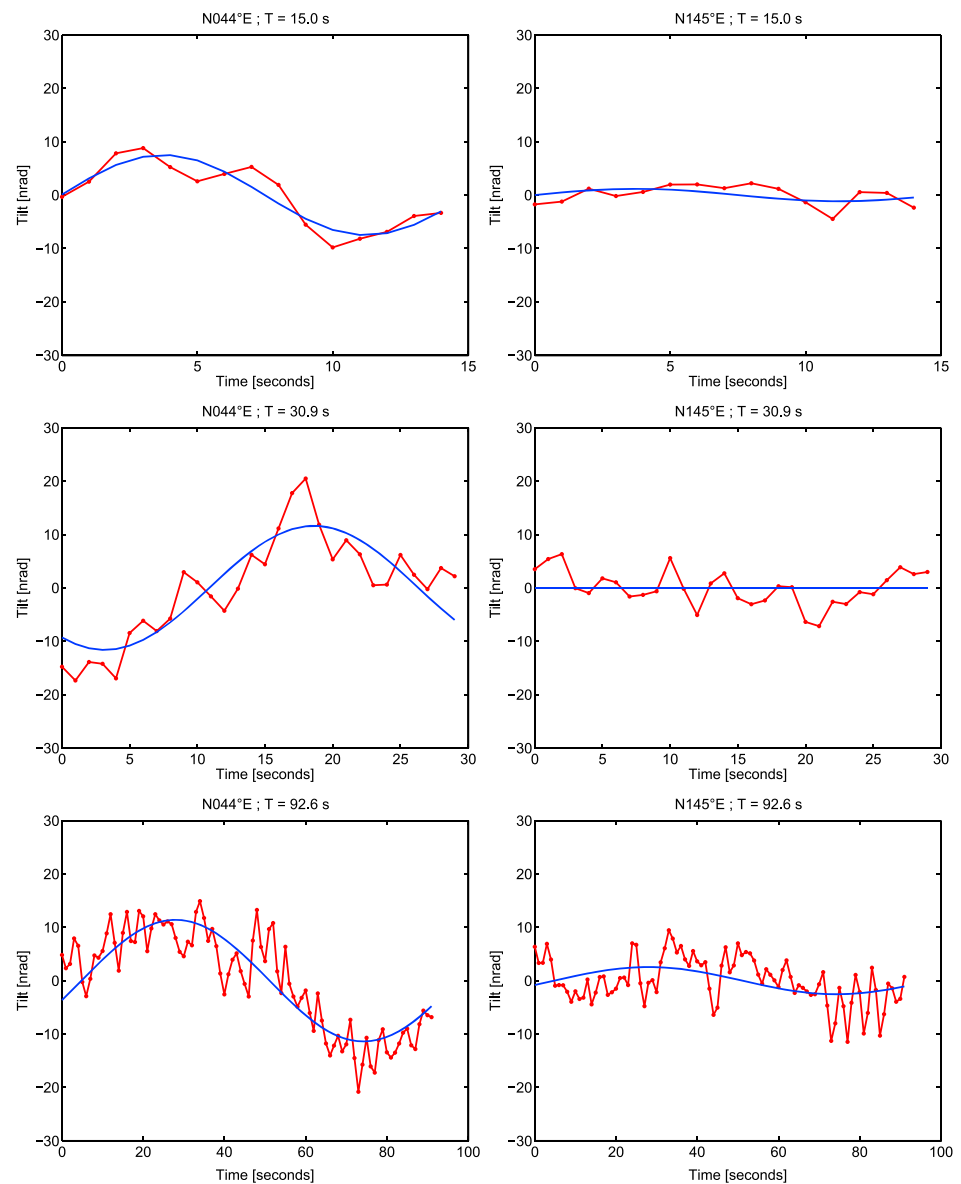


**Figure 9.** Stacked tiltmeter responses for three periodic hydromechanical tests performed on fracture B1-3 ( $d_f = 60.4$  m) in red and associated sine fit of amplitude  $\Theta$  and period  $T$  in blue.

oscillations and is exerted by each foot of the tripod onto the ground surface. In this section, we seek to investigate whether this effect can be recorded by our tiltmeters.

Assuming a semi-infinite elastic half-space, ground surface deformation caused by a normal force over a disk-shaped surface can be calculated analytically from the developments of *Farrell* [1972]. The 1-D problem requires the knowledge of the soil's elastic parameters, namely, Young's modulus  $E$  and Poisson's ratio  $\nu$ , as well as the distance to the load  $d_l$  and the disk's radius  $r_d$ , which here is fixed to 0.1 m and reveals negligible influence on tilt amplitude in this configuration (not shown here). Considering the problem's dimensions, we estimate that the norm of the force applied on each foot of the tripod is  $|F_s| \approx 18$  N. Unfortunately, as this effect was unforeseen, we did not precisely measure the distance between the tiltmeters and the tripod's feet. Seemingly, the mechanical properties of the soil are unknown but there is a way to estimate them if we know the response of a tiltmeter to a known mass placed at a known distance from it. This is where the individual passing by the tiltmeter during an experiment and seen in N44°E data (Figure 4a) comes into play. At that moment, this person weighted about 800 N and passed rapidly by the instruments, between the station and the closest foot of the tripod, hence at about 1.5 to 2 m from P1 (Figure 1). On the tilt signal, he created a

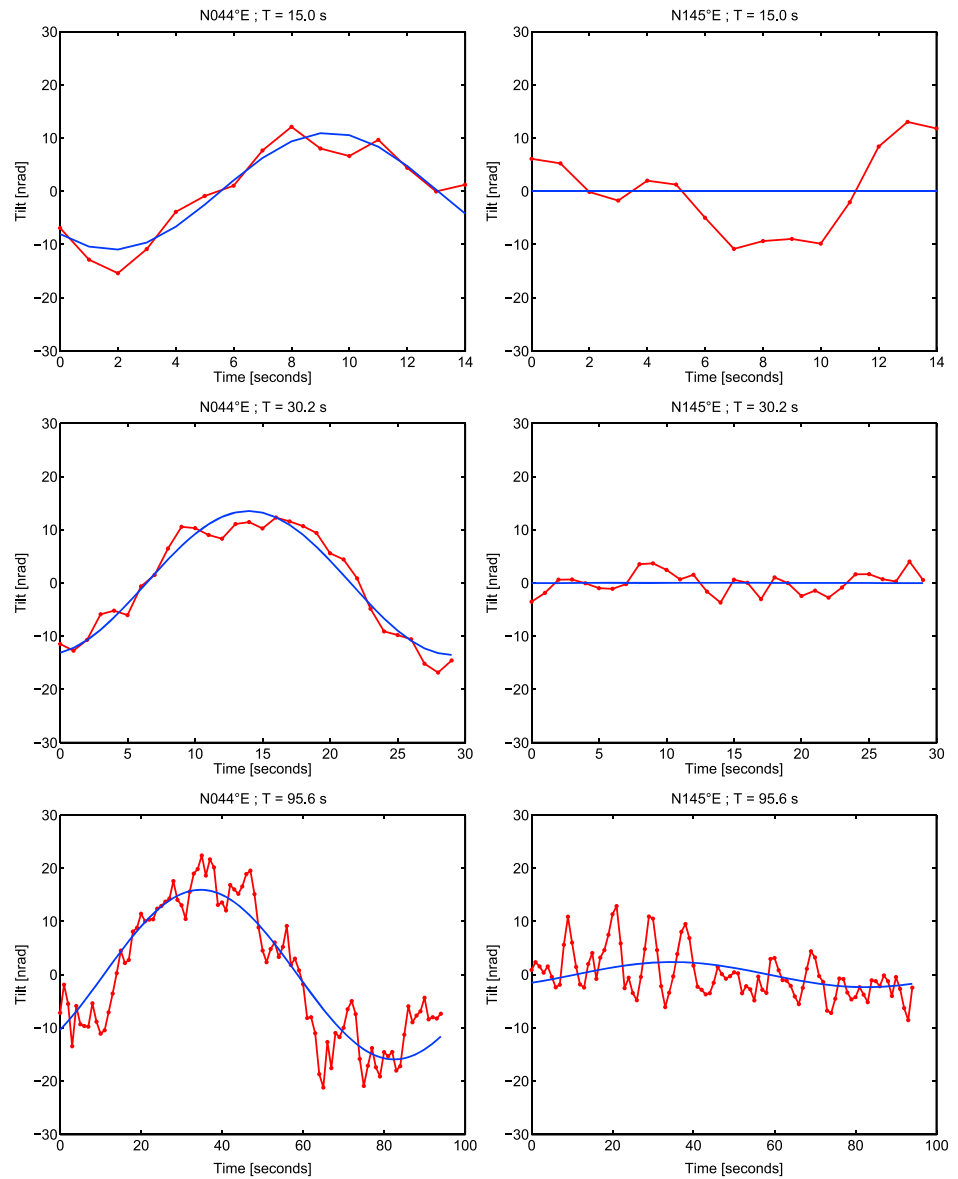


**Figure 10.** Stacked tiltmeter responses for three periodic hydromechanical tests performed on fracture B1-4 ( $d_f = 78.7$  m) in red and associated sine fit of amplitude  $\Theta$  and period  $T$  in blue.

decline of about  $420 \pm 20$  nrad (Figure 4). By fixing Poisson's ratio to  $\nu = 0.3$ , a widely used value for geotechnical applications, we estimate the soil's Young modulus  $E$  from Farrell's analytical solution [Farrell, 1972]. From Figure 11a, it appears that  $E$  should lie between 140 and 250 MPa, which is consistent for the humid sandy clay at this site. Using these values to calculate the tilt that the tripod would generate at the station, it seems that the buoyancy force alone cannot explain the observed tilt amplitudes (Figure 11b). We only consider the tripod foot closest to P1, given that the others are more than 3 m away from it and thus are unlikely to have any noticeable effect (Figures 1 and 11).

### 3.3. Assessing the Hydromechanical Effect

We define  $\Theta_{44}^*$ , the normalized stacked tilt amplitude of the N44°E instrument, as the ratio of tilt amplitude to fracture depth  $d_f$  and pressure amplitude in the chamber  $P_c$ :

$$\Theta_{44}^* = \frac{\Theta_{44}}{d_f P_c} \quad (9)$$

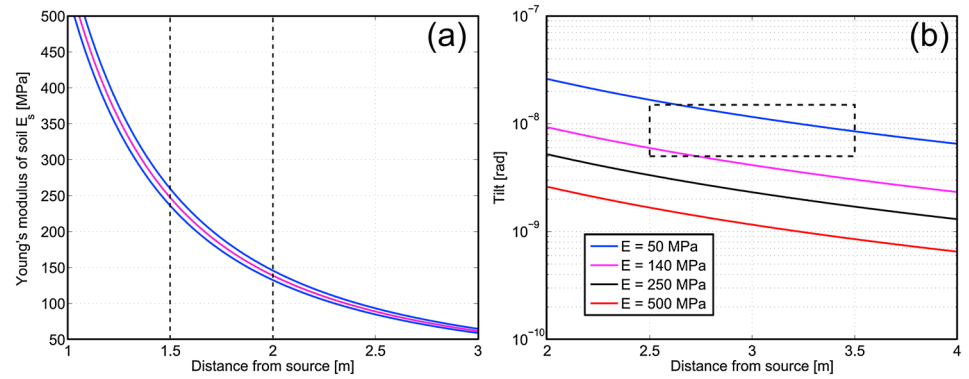


**Figure 11.** Evaluation of potential buoyancy effect on tilt data. (a) Recorded effect on the N44°E tiltmeter of an 82 kg individual (source) as a function of the soil's Young's modulus  $E_s = E$  and its distance to the instrument, calculated from the analytical solution of Farrell [1972]. The magenta and blue curves are the measured tilt amplitude (420 nrad) and its estimated confidence bounds ( $\pm 20$  nrad), respectively. The dashed vertical lines represent the approximate distance range at which a person passed by the tilt station P1; (b) calculated tilt profiles for N44°E corresponding to an applied force representative of one tripod foot's effect onto the ground surface, resulting from varying buoyancy force on the solid cylinder during a test, as a function of its distance from the tiltmeter. The different plain curves correspond to different soil Young's moduli  $E = E_s$  (Poisson's ratio is fixed at  $\nu = 0.3$ ). The dashed line rectangle is the area entailing our stacked tilt results.

In Figure 12 we display  $\Theta_{44}^*$  as a function of tested periods  $T$  on the three fractures. We discarded all tests with  $T > 120$  s considering the poor signal-to-noise ratios at these periods. This normalization allows for separating the mechanical behaviors of the three fractures. The normalized tilt amplitudes  $\Theta_{44}^*(T)$  for B1-4 (78.7 m) are significantly different from those for B1-2 and B1-3 (50.9 m and 60.4 m, respectively) as shown in Figure 12a. Furthermore, for each fracture  $\Theta_{44}^*(T)$  exhibits a weak dependency on  $T$  for periods  $T \geq 30$  s. For  $T \approx 15$  s, the normalized tilt amplitude is systematically higher than for other periods. We attributed this effect to resonance of the tiltmeter's pendulum. From equation (4) and as shown previously, one may infer that

$$\lim_{T \rightarrow T_0} G(T) = \frac{\Omega}{2\beta} \quad (10)$$

and

$$\lim_{T \rightarrow \infty} G(T) = \Omega \quad (11)$$

which demonstrate that the tiltmeter measures the actual ground motion  $\Omega$  for long external excitation periods  $T$ , but when the latter gets close to the eigen oscillation period of the tiltmeter  $T_0 \approx 9$  s, it experiences a resonance causing an amplification of the real perturbation by a factor  $(2\beta)^{-1}$  which is higher than 1 for  $\beta \leq 0.5$ . This function is reported in  $\Theta_{44}^*(T)$  graphs in Figure 12 (broken lines) with  $\beta = 0.1$  (dimensionless) and shows that this phenomenon explains well the decline of normalized tilt amplitude with increasing period (Figure 12).

Additionally, from the repeated tests (triplicates) on B1-4 (78.7 m) we observe that the experiments seem to be more repeatable for periods  $T \leq 70$  s. Therefore, we put more confidence in the results of short-period tests. Hence, we adjust the gain function  $G(T)$  to the normalized tilt amplitude  $\Theta_{44}^*(T)$  for short periods, so that we obtain the best estimate possible of the actual ground tilt  $\Omega$  in response to deep hydromechanical sources. In doing so, we obtain  $\Omega$  equal to 0.65, 0.45, and 3.2 nrad/m<sup>2</sup> for fractures B1-2, B1-3, and B1-4, respectively (Figure 12).

### 3.4. Fracture Properties

In periodic hydraulic tests, the characteristic penetration depth  $d_c$  of the pressure front into the formation and around the solicited well obeys approximately to a simple scaling law of the form [e.g., Renner and Messar, 2006]:

$$d_c \approx \sqrt{DT} \quad (12)$$

where  $D = T_h/S$  is the medium's hydraulic diffusivity. According to (12), the pressure front explores increasing fracture radii  $r_c = d_c$  for increasing periods of excitation  $T$ . Consequently for long-period hydraulic tests, a larger area of the tested fracture should undergo a change in effective stress and thus opening. Ultimately,

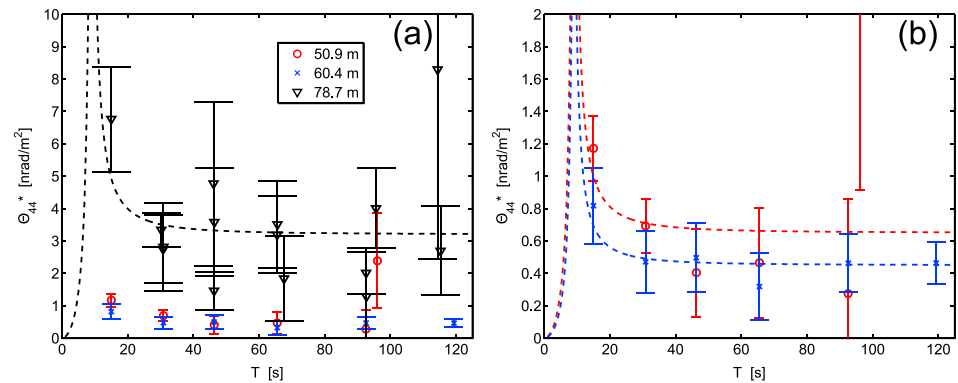


**Figure 12.** (a) Normalized amplitude of N44°E as a function of period  $T$  for each tested fracture, marked by their depth: B1-2 (50.9 m depth), B1-3 (60.4 m), and B1-4 (78.7 m). (b) Enlargement of Figure 12a to better visualize results of the two upper fractures' responses. The normalized amplitude  $\Theta_{44}^*$  is defined in equation (9) and the dashed lines represent  $G(T)$  functions defined in equation (4). Error bars correspond the RMSE of sine fits to the stacked tilt data: the width of an error bar is 2 times RMSE.

larger deforming fractures are likely to generate more observable ground surface deformation. Nonetheless, this intuitive reasoning does not match our observations because there is no perceptible dependency of normalized tilt on tested periods.

To explain this independency, a first hypothesis is that the change in tilt amplitude  $\Theta_{44}^*$  with period  $T$  is too small to be detected and falls within the measurement errors (see Figure 12). A second hypothesis is that during each hydraulic test, only a limited portion of the fracture is deformed, regardless of the penetration radius  $r_c$  of pressure perturbations. One effect that may cause such a behavior is the presence of important subvertical transmissive fractures intersecting the tested fractures isolated in borehole B1. Such effect was investigated by *Svenson et al.* [2007] and *Schweisinger et al.* [2011] who showed that a leakage (or fracture intersection) in a flat-lying fracture decreased the amplitude of fracture opening with increasing proximity to the injection point. A leakage should produce a pressure drop in the first fracture, as well as an important change in mechanical stress distribution. The presence of a well-connected fracture network at our site, involving permeable subvertical drains crossing the subhorizontal fractures of B1, was demonstrated by many previous studies [*Dorn et al.*, 2012, 2013; *Klepikova et al.*, 2014; *Le Borgne et al.*, 2007; *Shakas et al.*, 2016]. Another effect could be a sharp decrease in fracture compliance with distance from the well. Here we define as compliance  $C_f(x)$  the ratio of fracture normal opening  $\delta_a(x)$  to the applied change in effective stress (in Pa), which is due to fluid pressure variations  $P(x)$  in this study. The variable  $x$  refers to the horizontal distance from the borehole. Hence, for a horizontal fracture, we have

$$C_f(x) = \frac{\delta_a(x)}{P(x)} \quad (13)$$

The drilling operation and the repeated hydraulic tests on the site might have altered the mechanical properties of fractures in the immediate vicinity of the borehole, as observed, for example, from televiewer logs where they all appear with centimetric apertures (not shown here). This effect is also known and largely documented in the field of tunneling and results in what is called "excavation damaged zone" [*Rutqvist and Stephansson*, 2003]. Finally, one might also hypothesize that a combination of the three aforementioned effects produces the observed insensitivity of ground surface tilt to excitation period  $T$ .

We used a simple 2-D elastic model to provide a first insight on in situ fracture mechanical properties and geometry in the framework of our hydromechanical test (Figure 13). We considered a horizontal crack of length  $r_c$  embedded in an elastic, homogeneous, and isotropic domain with fixed Young's modulus ( $E = 20$  GPa) and Poisson's ratio ( $\nu = 0.3$ ). Besides, the crack is represented as a void in the formation, and its walls meet each other at the tip so that the compliance tends to zero close to this point. The fracture is located at 51 m below the free surface (Figure 13). The domain is rectangular in shape (300 m long  $\times$  200 m deep), and the mechanical boundary conditions are no motion in the horizontal and vertical directions for the far lateral edge and the bottom edge, respectively. Then, we tested three scenarios that represent end-member situations entailing our vision of the natural medium's properties at the site:

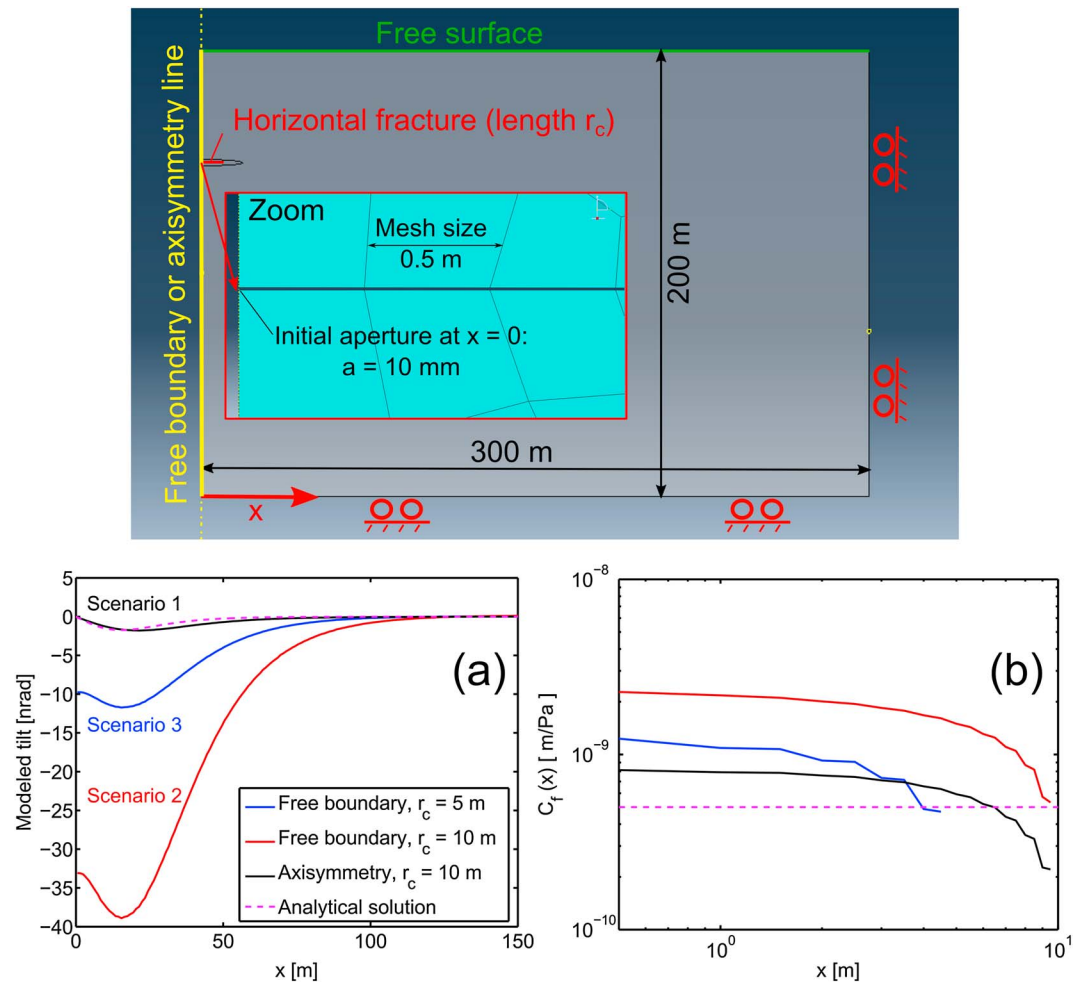


**Figure 13.** (top) Geometry and boundary conditions of the elastic model. The yellow left-hand boundary is either (1) a axisymmetric boundary (scenario 1) and (2) a free boundary (scenarios 2 and 3). (a) Surface tilt profiles obtained for different conditions. The analytical solution is from *Okada* [1985] and allows for calculating surface deformation from the uniform opening of a fracture plane in an elastic half-space. (b) Associated fracture compliance profiles.

1. A 10 m long fracture with axisymmetric mechanical boundary conditions at the edge from which the fracture emerges (Figure 13). This boundary condition is representative of the case where the crack is centered on the borehole.
2. A 10 m long fracture with free mechanical boundary conditions at the edge from which the fracture emerges. Such configuration approaches the conditions where the crack extends only on one side of the solicited borehole. In other words, it represents the most nonsymmetric case.
3. The last scenario reproduces scenario 2 with a 5 m long fracture. The chosen radii range (5 to 10 m) is in agreement with the interpretations of *Dorn et al.* [2013] who carried out borehole GPR experiments at the same test site.

Finally, we chose to apply an exponentially decreasing stress on the fractures' walls to approximate the effect of pressure diffusion into the crack, with

$$P(x) = P_c \exp(-x/r_c) \quad (14)$$

Here the driving pressure is set to  $P_c = 3000$  Pa in order to be close to the experimental conditions achieved for fracture B1-2 (Table 2).

The calculations show that no tilt could be theoretically detected at the surface in the axisymmetric case (scenario 1, Figure 13a). The resulting surface tilt profile in scenario 1 is close to the one obtained from classic analytical solutions for calculating surface deformation generated by a plane dislocation within a homogeneous elastic half-space [i.e., *Okada*, 1985], using the same geometry but assuming a uniformly applied

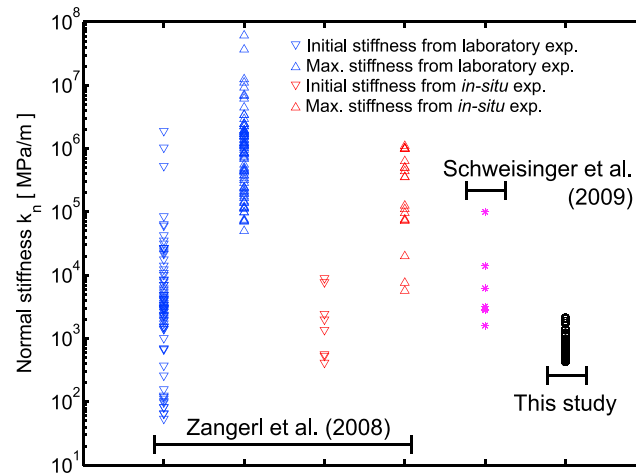


**Figure 14.** Comparison of different estimates of fracture normal stiffnesses  $k_n = C_f^{-1}$ . Zangerl et al. [2008] reviewed the results of several studies conducted either in laboratory or in the field. Schweisinger et al. [2009] performed in situ hydromechanical experiments on fractures at different depths ranging from 25 to 49 m.

pressure change against the fracture walls. On the other hand, when the domain boundary crossing the fracture is seen as an unconstrained boundary (scenarios 2 and 3), we observe surface tilt amplitudes about 10 times larger than in scenario 1 a few meters away from the solicited well, on the order of those measured on the field ( $\sim 10\text{--}30$  nrad, Figure 13a). Furthermore, we show the fracture compliance profiles  $C_f(x)$  for the various cases in Figure 13b. Surprisingly, all compliance values remain around the same order of magnitude along the fracture, especially in the first meters from the well (i.e.,  $\bar{C}_f \simeq 1 \times 10^{-9}$  m/Pa). The compliance consistently decreases toward the fracture’s tip in all scenarios. However, it decreases by a factor of  $\sim 8$  between borehole and fracture tip in the axisymmetric case, whereas it only falls by a factor of  $\sim 2$  in the free boundary case. Under these conditions, we remark that scenario 2 reproduces best the tilt amplitudes measured during the in situ hydromechanical experiment ( $\sim 10$  nrad at a point 4 m away from the borehole).

By taking an average compliance of  $\bar{C}_f \simeq 1 \times 10^{-9}$  m/Pa, reflecting the modeling results (Figure 13b), we may estimate fracture storativity  $S$  expressed as [Svenson et al., 2007]

$$S = \rho_w g (\bar{C}_f + aC_w), \quad (15)$$

where  $\rho_w$  and  $C_w$  are the water’s density and compressibility, respectively, and  $a$  is the fracture’s aperture. The term  $aC_w$  is generally negligible compared to  $\bar{C}_f$ , and with  $\rho_w g = 10^4$  N/m<sup>3</sup>, we obtain  $S \simeq 10^{-5}$  (dimensionless). This order of magnitude lies in the lower end of estimates from cross-borehole flowmeter test performed in the area by Le Borgne et al. [2006] but is higher than typical results from comparable hydromechanical field experiments [Burbey et al., 2012; Schweisinger et al., 2009; Svenson et al., 2008].

Seemingly, we computed the fracture normal stiffness  $k_n$  profiles for scenarios 2 and 3, simply given by  $k_n(x) = C_f(x)^{-1}$ , and compared them to data from the literature [i.e., Schweisinger et al., 2009; Zangerl et al., 2008, Figure 14]. Our results in terms of normal stiffness coincide with the lower bounds of laboratory and field data gathered in the review by Zangerl et al. [2008] for fractures in granitic rock. It is well known that fracture normal aperture increases with applied normal stress in a nonlinear fashion (typically, hyperbolic or logarithmic) [Rutqvist and Stephansson, 2003; Tsang and Witherspoon, 1981; Zangerl et al., 2008]. Hence, the fracture normal aperture variation first increases quickly for small changes in effective stress, but when the fracture is strongly stressed, the aperture variations become much smaller for any unit change in effective stress. The stiffness is given by the derivative of stress versus aperture function. Consequently, as our oscillating hydraulic test induced only small pressure variations, it is physically consistent that our estimates of stiffness fall in the lower range found in the literature.

#### 4. Discussion, Conclusion, and Perspectives

We presented a method to measure ground surface deformation associated to the pressurization of fractures at several depths. Here a combination of an oscillatory fluid pressure excitation of known frequency,

precise tiltmeters, and simple processing method offered the possibility to grasp deep hydromechanical phenomena of unprecedented small amplitudes. This first of its kind experiment has important implications for cost-effective studies of fractured media where contamination or similar issues may prevent from mobilizing large volumes of fluid as in pumping tests, or seemingly, where high pressurization of the medium is unsafe. Moreover, surface monitoring of ground deformation may be an interesting complement to closer *in situ* hydromechanical tests as in *Schweisinger et al.* [2009] and *Svenson et al.* [2008] given that the object is seen from a broader perspective.

However, performing and interpreting harmonic hydromechanical tests using tiltmeter data is not straightforward, especially in the presence of strong ambient noise. For example, the N145°E tiltmeter seemed to be blind to most hydromechanical processes stimulated by the oscillatory hydraulic test. In fact, this tiltmeter was equipped with a photoelectric cell more than twice less sensitive than its twin, which might partly explain its difficulty to monitor the targeted deformations. Nevertheless, we should recall that the amplitude estimate in the N145°E data is conditioned to a phase constraint that might also blur the interpretation to some extent. For instance, a sine fit could be found in the stacked data of N145°E for the 96 s test on B1-2 (Figure 8); instead, it shows a flat response because we are looking at a signal in phase with N44°E, based on the hypothesis of isotropic pressure diffusion. Here the chosen phase constraint may be disputable. Yet an absence of phase constraint in our case would result in erratic phase lags between the two instruments as a function of period  $T$ , which seems difficult to understand from a physical point of view. Hence, future developments using the same approach should treat this aspect with care to avoid losing information and also to be consistent with the mechanical processes that are studied.

The errors associated tilt amplitude estimation are relatively high but expectable given the conditions of the experiment, and the fact that we probably leaned against the very end of our method's detection limits. The experience acquired during our experiment should be beneficial to improve it in several ways. First, creating higher pressure amplitudes in the chamber should increase fracture deformation and thereby enhance detectability by tiltmeters. Second, all sources of instrument disturbance must be carefully avoided or, if it is not possible, as for wind effects, for instance, a way to better monitor side effects in the frequency domain could be implemented to subsequently filter them. Finally, one should use the same acquisition system for pressure and tilt records, to outrule any possible clock drifting artifacts that may introduce a severe bias in phase shift estimates between pressure and surface deformation.

Despite technicalities, we demonstrated the potential of the method to bring valuable information on a deep fracture's geometry and mechanical properties. The measured tilt amplitudes for sinusoidal hydraulic tests performed on three fractures showed no sensitivity to period  $T$ . A possible interpretation is that the pressure front is rapidly reaching an intersection between the solicited horizontal fracture and another more vertical one. Such leakage effect could dramatically decrease fracture deformation beyond the intersection. A way to test this hypothesis on the field would be to combine the harmonic hydromechanical test described in this paper, with geophysical methods which are sensitive to subsurface fluid paths like GPR [e.g., *Shakas et al.*, 2016] or self-potential data, already used in the periodic test framework by *Maineult et al.* [2008] and by *Soueid Ahmed et al.* [2016]. Furthermore, we were able to evidence the distinct mechanical responses of the three tested fractures at depth. Using a simple elastostatic model, we derived estimates of fracture stiffness and storativity that are consistent with the literature. These promising results should encourage further developments of the method, using for instance more tiltmeters at various locations and by adding strain instruments in boreholes. Future progress should also focus on more robust and extensive modeling to describe the sensitivity of surface tilt data to hydraulic, geometrical, and mechanical parameters under harmonic pumping conditions.

In addition, coupling oscillatory pressure tests and hydromechanical monitoring are likely to help understanding and quantifying *in situ* to what extent key parameters, such as fracture storativity, are varying depending on the stress state of the medium. *Vinci et al.* [2015] showed the importance of considering the fully coupled hydromechanical response of a fracture when interpreting pressure data of periodic pumping tests, in order to avoid significant biases in properties estimates. Besides, they demonstrated that the signature of hydromechanical effects could be easily distinguished in pressure patterns due to the periodic nature itself. Consequently, further work should gather efforts to combine knowledge from periodically induced pressure variations in fractures and their associated mechanical response, in order to both investigate nonstationarity of hydraulic properties and gain insight on *in situ* fracture mechanics.

## Notation

List of mathematical symbols, with signification and units.

Latin letters:

- $a$  fracture aperture (m),
- $C_f(x)$  fracture normal compliance at horizontal distance  $x$  from borehole (m/Pa),
- $C_w$  compressibility of water (Pa<sup>-1</sup>),
- $d_f$  fracture's depth in borehole B1 (m),
- $d_s$  diameter of the solid cylinder (m),
- $d_c$  characteristic penetration depth of the pressure front (m),
- $D$  hydraulic diffusivity (m<sup>2</sup>/s),
- $E$  Young's modulus of soil (Pa) also noted  $E_s$ ,
- $f_0$  eigenfrequency of a tiltmeter's pendulum (s<sup>-1</sup> or Hz),
- $f_c$  high-pass cutoff frequency (s<sup>-1</sup> or Hz),
- $f_s$  sampling frequency (s<sup>-1</sup> or Hz),
- $f_t$  frequency of harmonic in tilt signal (s<sup>-1</sup> or Hz),
- $F_s$  force applied by a tripod foot onto the soils' surface (N),
- $g$  gravity acceleration (s<sup>-1</sup> or Hz),
- $G(T)$  gain function,
  - $i$  imaginary unit defined as  $i^2 = -1$ ,
- $l(w)$  tiltmeter's transfer function,
- $k_n$  fracture normal stiffness (Pa/m),
- $K_p$  dimensionless constant,
- $l_s$  length of the solid cylinder (m),
- $n_p$  number of complete cylinder oscillations during a test,
- $N$  number of numbers in discrete sequence,
- $P$  fluid pressure (Pa or m),
- $P_c$  pressure amplitude in the chamber (Pa or m),
- $q$  pendulum's displacement (m),
- $r_c$  characteristic fracture radius (m),
- $S$  storativity (dimensionless),
- $t$  time (s),
- $T$  period of pressure oscillations in sealed chamber (s),
- $T_0$  eigenperiod of a tiltmeter's pendulum (s),
- $T_c$  high-pass cutoff period (s),
- $T_h$  transmissivity (m<sup>2</sup>/s),
- $T_t$  period of harmonic in tilt signal (s),
- $U$  differential output tension of a tiltmeter's photoelectric cells (mV),
- $x_n$   $n$ th number in sequence of length  $N$ ,
- $X_k$  discrete Fourier Transform of  $x_n$ .

Greek letters:

- $\beta$  relative dampening coefficient (dimensionless),
- $\delta_a(x)$  fracture mode I (normal) opening at a distance  $x$  from the borehole (m),
- $\Gamma$  amplification factor of a tiltmeter (mV/rad/s<sup>2</sup>),
- $\nu$  Poisson's ratio (dimensionless),
- $\omega$  pulsation (s<sup>-1</sup> or Hz),
- $\omega_0$  eigenpulsation of a tiltmeter's pendulum (s<sup>-1</sup> or Hz),
- $\Omega$  ground surface tilt (rad),
- $\Omega_{44}^*$  normalized stacked tilt amplitude recorded by N44°E instrument (nrad/m<sup>2</sup>),
- $\phi$  tiltmeter orientation with respect to the North (°),
- $\varphi$  phase (rad),
- $\rho_w$  water density (kg/m<sup>3</sup>),
- $\sigma_\theta$  standard deviation of tilt amplitudes (nrad),

- $\theta$  measured tilt signal (rad),  
 $\Theta_\phi$  amplitude of stacked tilt data from tiltmeter with orientation  $N\phi^\circ E$  (nrad),  
 $\Upsilon(f_i)$  amplitude spectral density (nrad).

### Acknowledgments

This work is part of the ANR project EQUIPEX CRITEX (grant ANR-11-EQPX-0011), with a combination of work packages 2.2 and 7.2, from which it has mainly been supported. Part of the scientific equipment has been purchased through the H+ observatory network. J. Schuite's PhD thesis is partly funded by the Brittany Region. Tilt data are available upon request at <http://hplus.ore.fr/>. We warmly thank Joerg Renner and two anonymous reviewers for providing insightful comments and suggestions that largely improved the quality of the paper. The Editor A. Revil is also sincerely acknowledged for handling the review process with care. Discussions with Nicolas Florsch were greatly appreciated.

### References

- Agnew, D. C. (1986), Strainmeters and tiltmeters, *Rev. Geophys.*, *24*(3), 579–624.
- Baker, C. J. (1997), Measurements of the natural frequencies of trees, *J. Exp. Bot.*, *48*(310), 1125–1132.
- Bakhos, T., M. Cardiff, W. Barrash, and P. K. Kitanidis (2014), Data processing for oscillatory pumping tests, *J. Hydrol.*, *511*, 310–319.
- Bandis, S. C., A. C. Lumsden, and N. R. Barton (1983), Fundamentals of rock joint deformation, *Int. J. Rock Mech. Min. Sci. Geomech. Abstr.*, *20*(6), 249–268.
- Barton, N. R., S. C. Bandis, and K. Bakhtar (1985), Strenght, deformation and conductivity coupling of joints, *Int. J. Rock Mech. Min. Sci. Geomech. Abstr.*, *22*(3), 121–140.
- Becker, M. W., and A. M. Shapiro (2000), Tracer transport in fractured crystalline rock: Evidence of nondiffusive breakthrough tailing, *Water Resour. Res.*, *36*(7), 1677–1686, doi:10.1029/2000WR900080.
- Ben Maamar, S., L. Aquilina, A. Quaiser, H. Pauwels, S. Michon-Coudouel, V. Vergnaud-Ayraud, T. Labasque, C. Roques, B. W. Abbott, and A. Dufresne (2015), Groundwater isolation governs chemistry and microbial community structure along hydrologic flowpaths, *Front. Microbiol.*, *6*, 1457.
- Berkowitz, B. (2002), Characterizing flow and transport in fractured geological media: A review, *Adv. Water Resour.*, *25*, 861–884.
- Bonnet, E., O. Bour, N. E. Odling, P. Davy, I. Main, P. Cowie, and B. Berkowitz (2001), Scaling of fracture systems in geological media, *Rev. Geophys.*, *39*(3), 347–383.
- Boussinesq, J. (1868), Mémoire sur l'influence des frottements dans les mouvements réguliers des fluides, *J. Liouville*, *13*, 377–424.
- Burbey, T. J., D. Hisz, L. C. Murdoch, and M. Zhang (2012), Quantifying fractured crystalline-rock properties using well tests, earth tides and barometric effects, *J. Hydrol.*, *414–415*, 317–328.
- Cappa, F., Y. Guglielmi, S. Graffet, H. Lançon, and I. Lamarque (2006), Use of in situ fiber optic sensors to characterize highly heterogeneous elastic displacement fields in fractured rocks, *Int. J. Rock Mech. Min. Sci.*, *43*(4), 647–654.
- Cappa, F., Y. Guglielmi, J. Rutqvist, C.-F. Tsang, and A. Thoraval (2006b), Hydromechanical modeling of pulse tests that measure both fluid pressure and fracture-normal displacement of the Coaraze Laboratory site, France, *Int. J. Rock Mech. Min. Sci.*, *43*, 1062–1082.
- Cardiff, M., T. Bakhos, P. K. Kitanidis, and W. Barrash (2013), Aquifer heterogeneity characterization with oscillatory pumping: Sensitivity analysis and imaging potential, *Water Resour. Res.*, *49*, 5395–5410, doi:10.1002/wrcr.20356.
- Cornet, F. H. (2016), Seismic and aseismic motions generated by fluid injections, *Geomech. Energy Env.*, *5*, 42–54.
- De Dreuzy, J.-R., P. Davy, and O. Bour (2001a), Hydraulic properties of two-dimensional random fracture networks following a power law length distribution: 1. Effective connectivity, *Water Resour. Res.*, *37*(8), 2065–2078.
- De Dreuzy, J.-R., P. Davy, and O. Bour (2001b), Hydraulic properties of two-dimensional random fracture networks following a power law length distribution: 2. Permeability of networks based on lognormal distribution of apertures, *Water Resour. Res.*, *37*(8), 2079–2095.
- Dorn, C., N. Linde, T. Le Borgne, O. Bour, and M. Klepikova (2012), Inferring transport characteristics in a fractured rock aquifer by combining single-hole ground-penetrating radar reflection monitoring and tracer test data, *Water Resour. Res.*, *48*, W11521, doi:10.1029/2011WR011739.
- Dorn, C., N. Linde, T. Le Borgne, O. Bour, and J.-R. De Dreuzy (2013), Conditioning of stochastic 3-D fracture networks to hydrological and geophysical data, *Adv. Water Resour.*, *62*, 79–89.
- Evans, K., and F. Wyatt (1984), Water table effects on the measurement of earth strain, *Tectonophysics*, *108*, 323–337.
- Farrell, W. E. (1972), Deformation of the Earth by surface loads, *Rev. Geophys.*, *10*(3), 761–797.
- Florsch, N., H. Legros, and J. Hinderer (1995), The search for weak harmonic signals in a spectrum with application to gravity data, *Phys. Earth Planet. Inter.*, *90*(3–4), 197–210.
- Guiltinan, E., and M. W. Becker (2015), Measuring well hydraulic connectivity in fractured bedrock using periodic slug tests, *J. Hydrol.*, *521*, 100–107.
- Guglielmi, Y., F. Cappa, and D. Amitrano (2008), High-definition analysis of fluid-induced seismicity related to the mesoscale hydromechanical properties of a fault zone, *Geophys. Res. Lett.*, *35*, L06306, doi:10.1029/2007GL033087.
- Guglielmi, Y., F. Cappa, J.-P. Avouac, P. Henry, and D. Elsworth (2015), Seismicity triggered by fluid injection-induced aseismic slip, *Science*, *348*(6240), 1224–1226.
- Hisz, D. B., J. C. Murdoch, and L. N. Germanovich (2013), A portable borehole extensometer and tiltmeter for characterizing aquifers, *Water Resour. Res.*, *49*, 7900–7910, doi:10.1002/wrcr.20500.
- Klepikova, M. V., T. Le Borgne, O. Bour, K. Gallagher, R. Hochreutener, and N. Lavenant (2014), Passive temperature tomography experiments to characterize transmissivity and connectivity of preferential flow paths in fractured media, *J. Hydrol.*, *512*, 549–562.
- Le Borgne, T., O. Bour, F. L. Paillet, and J.-P. Caudal (2006), Assessment of preferential flow path connectivity and hydraulic properties at single-borehole and cross-borehole scales in a fractured aquifer, *J. Hydrol.*, *328*, 347–359.
- Le Borgne, T., et al. (2007), Comparison of alternative methodologies for identifying and characterizing preferential flow paths in heterogeneous aquifers, *J. Hydrol.*, *345*, 134–148.
- Le Goc, R., J.-R. De Dreuzy, and P. Davy (2010), An inverse problem methodology to identify flow channels in fractured media using synthetic steady-state head and geometrical data, *Adv. Water Resour.*, *33*(7), 782–800.
- Maineult, A., E. Strobach, and J. Renner (2008), Self-potential signals induced by periodic pumping tests, *J. Geophys. Res.*, *113*, B01203, doi:10.1029/2007JB005193.
- Manga, M., I. Beresnev, E. E. Brodsky, J. E. Elkhoury, D. Elsworth, S. E. Ingebritsen, D. C. Mays, and C.-Y. Wang (2012), Changes in permeability caused by transient stresses: Field observations, experiments, and mechanisms, *Rev. Geophys.*, *50*, RG2004, doi:10.1029/2011RG000382.
- Mann, J., R. Jäger, T. Müller, G. Höcht, and P. Hubral (1999), Common-reflection-surface stack—A real data example, *J. Appl. Geophys.*, *42*(3–4), 301–318.
- Mayne, W. H. (1962), Common reflection point horizontal data stacking techniques, *Geophysics*, *27*(6), 927–938.
- Murdoch, L. C., and L. N. Germanovich (2012), Storage change in a flat-lying fracture during well tests, *Water Resour. Res.*, *48*, W12528, doi:10.1029/2011WR011571.
- Neuman, S. P. (2005), Trends, prospects and challenges in quantifying flow and transport through fractured rocks, *Hydrogeol. J.*, *13*, 124–147.
- Okada, Y. (1985), Surface deformation due to shear and tensile faults in a half-space, *Bull. Seismol. Soc. Am.*, *75*(4), 1135–1154.

- Pedersen, K. (1997), Microbial life in deep granitic rock, *FEMS Microbiol. Rev.*, *20*, 399–414.
- Renner, J., and M. Messar (2006), Periodic pumping tests, *Geophys. J. Int.*, *167*, 479–493.
- Renshaw, C. E. (1995), On the relationship between mechanical and hydraulic apertures in rough-walled fractures, *J. Geophys. Res.*, *100*(B12), 24,629–24,636.
- Rice, J. R., and M. P. Cleary (1976), Some basic stress diffusion solutions for fluid saturated elastic porous media with compressible constituents, *Rev. Geophys.*, *14*, 227–241.
- Roeloffs, E. A. (1988), Fault stability changes induced beneath a reservoir with cyclic variations in water level, *J. Geophys. Res.*, *93*(B3), 2107–2124.
- Rutqvist, J. (2015), Fractured rock stress-permeability relationships from in situ data and effects of temperature and chemical-mechanical couplings, *Geofluids*, *15*(1–2), 48–66.
- Rutqvist, J., and O. Stephansson (2003), The role of hydromechanical coupling in fractured rock engineering, *Hydrogeol. J.*, *11*, 7–40.
- Rutqvist, J., J. Noorishad, C.-F. Tsang, and O. Stephansson (1998), Determination of fracture storativity in hard rocks using high-pressure injection testing, *Water Resour. Res.*, *34*(10), 2551–2560.
- Saleh, J., P. A. Blum, and H. Delorme (1991), New silica compact tiltmeter for deformations measurement, *J. Surv. Eng.*, *117*(1), 27–35.
- Schimmel, M., and H. Paulssen (1997), Noise reduction and detection of weak, coherent signals through phase-weighted stacks, *Geophys. J. Int.*, *130*(2), 497–505.
- Schuite, J., L. Longuevergne, O. Bour, F. Boudin, S. Durand, and N. Lavenant (2015), Inferring field-scale properties of a fractured aquifer from ground surface deformation during a well test, *Geophys. Res. Lett.*, *42*, 10,696–10,703, doi:10.1002/2015GL066387.
- Schweisinger, T., L. C. Murdoch, and C. Huey (2007), Removable borehole extensometers for measuring axial displacements during well tests, *Geotech. Test. J.*, *30*(3), 202.
- Schweisinger, T., E. J. Svenson, and L. C. Murdoch (2009), Introduction to hydromechanical well tests in fractured rock aquifers, *Ground Water*, *47*(1), 69–79.
- Schweisinger, T., E. J. Svenson, and L. C. Murdoch (2011), Hydromechanical behavior during constant-rate pumping tests in fractured gneiss, *Hydrogeol. J.*, *19*, 963–980.
- Segall, P. (1992), Induced stresses due to fluid extraction from axisymmetric reservoirs, *Pure Appl. Geophys.*, *139*(3–4), 535–560.
- Shapiro, A. M., and P. A. Hsieh (1998), How good are estimates of transmissivity from slug tests in fractured rock?, *Ground Water*, *36*(1), 37–48.
- Shakas, A., N. Linde, L. Baron, O. Bochet, O. Bour, and T. Le Borgne (2016), Hydrogeophysical characterization of transport processes in fractured rock by combining push-pull and single-hole ground penetrating radar experiments, *Water Resour. Res.*, *52*, 938–953, doi:10.1002/2015WR017837.
- Slack, T. Z., L. C. Murdoch, L. N. Germanovich, and D. B. Hisz (2013), Reverse water-level change during interference slug tests in fractured rock, *Water Resour. Res.*, *49*, 1552–1567.
- Soueid Ahmed, A., A. Jardani, A. Revil, and J. P. Dupont (2016), Joint inversion of hydraulic head and self-potential data associated with harmonic pumping tests, *Water Resour. Res.*, *52*, 6769–6791, doi:10.1002/2016WR019058.
- Svenson, E., T. Schweisinger, and L. C. Murdoch (2007), Analysis of the hydromechanical behavior of a flat-lying fracture during a slug test, *J. Hydrol.*, *347*, 35–47.
- Svenson, E., T. Schweisinger, and L. C. Murdoch (2008), Field evaluation of the hydromechanical behavior of flat-lying fracture during slug tests, *J. Hydrol.*, *359*, 30–45.
- Tsang, Y. W., and P. A. Witherspoon (1981), Hydromechanical behavior of a deformable rock fracture subject to normal stress, *J. Geophys. Res.*, *86*(B10), 9287–9298.
- Vinci, C., H. Steeb, and J. Renner (2015), The imprint of hydro-mechanics of fractures in periodic pumpings tests, *Geophys. J. Int.*, *202*, 1613–1626.
- Witherspoon, P. A., J. S. Y. Wang, K. Iwai, and J. E. Gale (1980), Validity of cubic law for fluid flow in a deformable rock fracture, *Water Resour. Res.*, *16*(6), 1016–1024.
- Wang, H. F. (2000), *Theory of Linear Poroelasticity With Applications to Geomechanics and Hydrogeology*, Princeton Univ. Press, Princeton, N. J.
- Wang, L., and M. B. Cardenas (2016), Development of an empirical model relating permeability and specific stiffness for rough fractures from numerical deformation experiments, *J. Geophys. Res. Solid Earth*, *121*, 4977–4989, doi:10.1002/2016JB013004.
- Zangerl, C., K. F. Evans, E. Eberhardt, and S. Loew (2008), Normal stiffness of fractures in granitic rock: A compilation of laboratory and in-situ experiments, *Int. J. Rock Mech. Min.*, *45*, 1500–1507.